PHYSICAL REVIEW RESEARCH **6**, L012029 (2024)

Letter

Adsorption superlattice stabilized by elastic interactions in a soft porous crystal

Kota Mitsumoto[*] and Kyohei Takae[†]
Department of Fundamental Engineering, Institute of Industrial Science, University of Tokyo,
4-6-1 Komaba, Meguro-ku, Tokyo 153-8505, Japan

(Received 14 September 2023; accepted 9 January 2024; published 16 February 2024)

Elasticity is essential for organizing mesoscale patterns in condensed matter. Here, we numerically show that adsorbed molecules in soft porous crystals form a superlattice (SL) stabilized by elastic interactions. In a mechanically flexible honeycomb lattice model, a long-range ordered 1/3-filling SL state emerges during adsorption. The SL state is robust against thermal fluctuation when the elastic interactions between the next-nearest-neighboring lattice sites are strong. Our results provide a way to switch the functionalities of materials by controlling the distribution of adsorbed molecules.

DOI: 10.1103/PhysRevResearch.6.L012029

Metal-organic frameworks (MOFs) are crystalline compounds consisting of inorganic nodes and organic linkers, whose numerous combinations enable us to design their functions such as porosity, elasticity, and electronic properties [1–3]. In particular, their potential application as a porous material has attracted much attention because of their large internal surface area and adsorption selectivity, which are utilized for gas separation/storage [4], sensors [5], catalysis [6], and biomedicines [7]. MOFs having mechanically flexible frameworks, called soft porous crystals (SPCs) [1,8], exhibit mechanical deformation with a change of the elastic moduli upon gas adsorption [9–12]. Utilizing the mechanical flexibility of the host matrix, SPCs show adsorption-desorption transitions with strong hysteresis and multistep adsorption isotherms [13–18], which are beneficial properties to control stably the amount of adsorption.

Another consequence of mechanical flexibility is the controllability of the spatial distribution of guest adsorbates. In particular, some SPCs exhibit a superlattice (SL) formation upon molecular adsorption. In IRMOF-74-V-hex [19,20] and $\mathrm{Co_2(dobdc)}$ [21,22], it was shown by x-ray diffraction measurements and molecular dynamics (MD) simulations that heterogeneous lattice distortion couples with heterogeneous guest distribution, resulting in the formation of a 2×2 SL structure. Although guest-induced local framework distortion has been studied, however, the role of a long-range guest-guest interaction mediated by the framework's elasticity remains elusive. As shown in other condensed matter exhibiting SL structures, such as nanoparticle quantum dots [23–27], plasmonic SLs [28], and phononic crystals [29], the long-range elastic interaction determines the mesoscopic structural formation [25,30–33]. In these substances, controlling the SL structure is important in enhancing the thermoelectric, optoelectric, and phononic properties [23,27,29]. Thus, it should be informative also in SPCs, both from condensed matter physics and practical applications, to reveal the role of the elasticity-mediated guest-guest interaction leading to a SL structure.

To examine numerically the long-range nature of the elastic interaction in SPCs, vast computational costs are required if guest molecules and a deformable host matrix are fully incorporated. Thus, a coarse-grained lattice model is needed to elucidate the role of elasticity in SPCs with manageable computational costs. The present authors have constructed a coarse-grained square lattice model, incorporating adsorption-induced lattice expansion/contraction and hardening/softening [34]. Elucidating the connection of the spatial guest distribution with thermodynamics, it has been found that spatial heterogeneity in the stiffness of host frameworks (elastic heterogeneity) leads to a hysteretic adsorption-desorption transition. Extending the coarse-grained model to the honeycomb lattice, where SL structures are observed experimentally [19,21,22], allows us to investigate the mechanism of SL formations in SPCs.

In this Letter, we present that an adsorbate SL structure is stabilized by an elasticity-mediated guest-guest interaction in SPCs. We consider a coarse-grained honeycomb lattice model which incorporates the adsorption-induced lattice expansion and hardening. The lattice sites interact with the nearest-neighbor (NN) and next-nearest-neighbor (NNN) sites via a simple spring potential. We reveal that elastic heterogeneity leads to the robust hysteresis in the case of the square lattice case [34] but, in contrast, a $\sqrt{3} \times \sqrt{3}$ (1/3-filling) SL state emerges, whose structure is different from the one observed experimentally [19,21,22]. The SL state is stabilized by NNN elastic interactions. When the NNN elastic interaction is sufficiently strong, the adsorption fraction exhibits a 1/3 plateau during the adsorption process in a certain parameter region, while there is no intermediate plateau during the desorption

---

[*] kmitsu@iis.u-tokyo.ac.jp
[†] takae@iis.u-tokyo.ac.jp

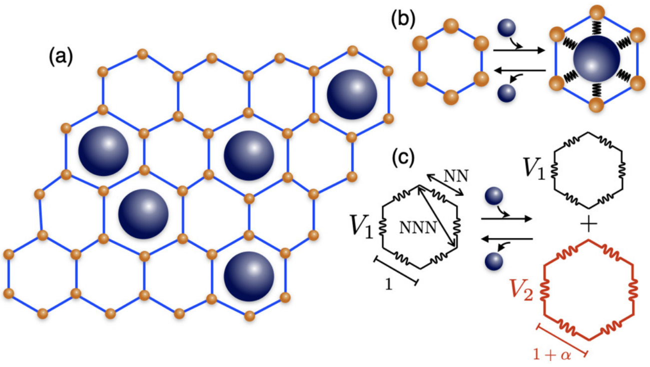

FIG. 1. Schematic description of the proposed model. (a) Guest particles (dark blue spheres) are adsorbed into the host honeycomb matrix formed by the host particles (orange), inducing isotropic swelling of the host matrix locally. (b) An adsorbed particle strongly interacts with the host particles. (c) Mathematical representation of (a) and (b). Interaction potential V_2 arises from the filling of the guest particle in addition to the original host's potential V_1.

process. Correspondingly, the free-energy landscape against the fraction of adsorbed sites takes a local minimum at 1/3, which implies that the SL state is robust against thermal fluctuations. Our findings provide a physical mechanism to realize the SL structure, which can be utilized for controlling the spatial distribution of adsorbed particles.

In experiments, honeycomb MOFs exhibiting an adsorption SL have a three-dimensional structure, with each hexagon forming a one-dimensional channel in the direction perpendicular to the honeycomb plane [19,21,22]. The structural change with respect to the direction of the channel is much smaller than the one in the honeycomb plane upon adsorption. Therefore, we construct a flexible two-dimensional honeycomb lattice, as shown in Fig. 1(a), whose lattice sites interact with the NN and NNN sites. The NN and NNN potentials of distance r are $\frac{k_0}{2}(l_0 - r)^2$ and $\frac{gk_0}{2}(\sqrt{3}l_0 - r)^2$, respectively, where k_0 and l_0 are the elastic constants and the natural length of the unit hexagon, and g is the ratio of the NNN interaction to the NN interaction. Hereafter, we adopt l_0 and $k_0 l_0^2$ as units of length and energy, respectively. Thus, the potential energy of the unit cell is given by $V_1(\{\boldsymbol{r}_{i\in\hexagon}\}) = \frac{1}{4}\sum_{\mathrm{NN}}(1 - r_{ij})^2 + \frac{g}{2}\sum_{\mathrm{NNN}}(\sqrt{3} - r_{ij})^2$, where $\{\boldsymbol{r}_{i\in\hexagon}\}$ represents the positions of the lattice sites forming the hexagon $\hexagon$. Each hexagonal unit cell can accommodate only one guest particle. Then the hexagon favors expanding isotropically by the interaction between the guest particle and host matrix, as shown in Fig. 1(b). This interaction is expressed as an additional potential energy $V_2(\{\boldsymbol{r}_{i\in\hexagon}\}) = k[\frac{1}{4}\sum_{\mathrm{NN}}(1 + \alpha - r_{ij})^2 + \frac{g}{2}\sum_{\mathrm{NNN}}(\sqrt{3}(1+\alpha) - r_{ij})^2]$, where k is the relative energy scale of the guest-host interaction, and α is a swelling parameter, as shown in Fig. 1(c). Thus, the equilibrium lattice constant and rigidity of a hexagon adsorbing a guest particle are $1 + k\alpha/(1+k)$ and $1 + k$, respectively. Each hexagon expands/contracts by adsorbing a guest if $k\alpha$ is positive/negative. The sign of k determines whether the hexagons harden or soften. In this study, we use a fixed parameter set $k = 3$ and $\alpha = 0.4$.

In this study, we adopt an osmotic ensemble [35], whose control parameters are the temperature T, the chemical potential of the guest particle adsorption μ, the number of host matrix sites N_{host}, and the hydrostatic pressure P. The osmotic grand potential is defined as $\Omega = U - TS + PV - \mu N_{\mathrm{ads}}$, where U is the internal energy, S is the entropy, V is the volume, and N_{ads} is the number of adsorption particles. In this study, we fix $N_{\mathrm{host}} = 2L^2$, where L is the linear system size of the honeycomb lattice. Thus, the lattice site positions $\boldsymbol{r}_i$ ($i = 1, 2, \dots, 2L^2$) on the honeycomb lattice with a periodic boundary condition and guest variables on the hexagons $\sigma_{\hexagon}$ ($\hexagon = 1, 2, \dots, L^2$) taking 1 (presence) or 0 (absence) follow the Hamiltonian given by

$$\mathcal{H} = \sum_{\hexagon=1}^{L^2} [V_1(\{\boldsymbol{r}_{i\in\hexagon}\}) + \sigma_{\hexagon}[V_2(\{\boldsymbol{r}_{i\in\hexagon}\}) - \mu]] + PV. \tag{1}$$

Note that the guest variables are on the dual lattice of the honeycomb lattice, i.e., a triangular lattice. Hence, the maximum number of adsorbed particles is half of N_{host}. We fix the hydrostatic pressure $P = 0.5$. The weak pressure stabilizes an SL state because the SL state has a lower volume than a fully adsorbed state. Indeed, our model does not exhibit the 1/3-filling SL state at $P = 0.0$ (see Supplemental Material Fig. S1 [36]). It should also be mentioned that high pressure breaks the honeycomb structure of the host matrix. We perform standard Monte Carlo (MC) simulations for $L = 12$–72 to investigate the hysteretic adsorption-desorption transition and multicanonical MC simulations using the Wang-Landau (WL) method for $L = 12$ to study the equilibrium phase transition and free-energy landscapes (see also Supplemental Material [36]).

Figures 2(a) and 2(b) show the μ-T phase diagrams at $P = 0.5$ with the ratio of the NNN interaction to the NN interaction $g = 1$ and $g = 2$, respectively. In the case of $g = 1$, adsorbed and desorbed states are realized in the red and blue regions, respectively, independent of the simulation protocols. Hysteretic behavior is observed in the yellow region. The equilibrium phase boundary is obtained by the WL simulations, crossing the middle of the hysteretic region. Thus, the adsorbed (desorbed) states are not thermodynamically stable below (above) the equilibrium phase boundary in the yellow region. The phase behavior is quite similar to the square lattice case (see Fig. 2 in Ref. [34]). In contrast, in the case of $g = 2$ [Fig. 2(b)], a 1/3-filling SL state forming a triangular lattice emerges by crossing the dark gray region in the cooling protocol. The 1/3-filling SL state has a $\sqrt{3} \times \sqrt{3}$ unit cell compared to the one of the original triangular lattice, as shown in Fig. 2(c). Snapshots of the whole system are shown in Supplemental Material Fig. S2 [36]. The adjacent sites of an adsorbed site are desorbed, and the NNN sites are adsorbed except for defects due to thermal fluctuation. The SL state stably holds as long as the system does not deviate from the light and dark gray regions by heating or decreasing μ. Thus, hysteresis between desorbed and SL states is observed.

Now, we investigate the reason why the 1/3-filling SL state is stabilized. Because the elastic energy depends on configurations of adsorbed sites, effective interactions between guest particles mediated by the elasticity of the host matrix emerge.

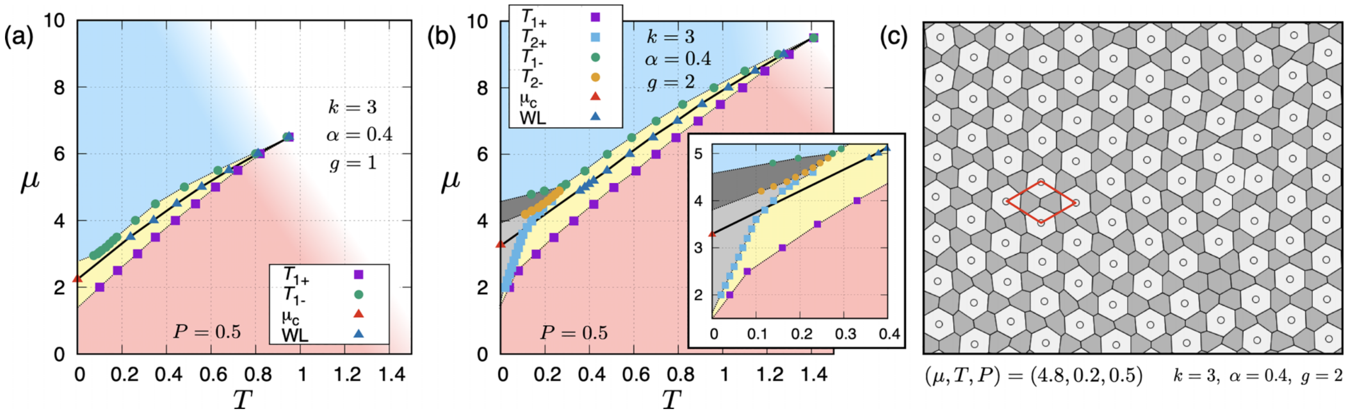

FIG. 2. Phase diagram of the model at $P = 0.5$ with $k = 3$, $\alpha = 0.4$, and the ratio of NNN interaction to the NN interaction, (a) $g = 1$ and (b) $g = 2$. The solid curve represents the equilibrium phase boundary between the adsorbed and desorbed phases, determined from the specific-heat peaks obtained by the WL method. The transition point at $T = 0$ is analytically determined by comparing the minimum energy of the desorbed and adsorbed states. The boundaries between different colors are determined from the specific-heat peaks obtained by quasiequilibrium protocols: T_{1+} and T_{2+} represent transition points to the desorbed state and $\sqrt{3} \times \sqrt{3}$ (1/3-filling) SL state during a heating process, and T_{1-} and T_{2-} represent transition points to the adsorbed state and 1/3-filling SL state during a cooling process. The inset shows a zoom of the region where the SL state appears. (c) A snapshot of a 1/3-filling SL state at $(\mu, T, P) = (4.8, 0.2, 0.5)$ with $k = 3$, $\alpha = 0.4$, and $g = 2$. Light gray hexagons with circles and dark gray hexagons represent adsorbed and desorbed sites, respectively. Short-time averaging over 1000 MC steps with a fixed adsorbate distribution is performed to obtain the average lattice distortion. Red lines represent a unit cell of the SL.

Figure 3(a) displays the enthalpy increase of each local configuration per site Δh from the ground state at $(\mu, P) = (0, 0.5)$ for $g = 1$ [the case of $g = 2$ is presented in Supplemental Material Figs. S3(a)–S3(c) [36]]. The enthalpy is increased by 2.75 due to an isolated adsorbed site (i). Forming a dimer (ii) or trimer [(v), (vi)] cluster, the enthalpy increases by 0.1–0.2 per site compared to two isolated adsorbed sites. The trimer tends to be isotropic because the adsorbed cluster is harder than the surrounding desorbed sites, which is a well-known feature of elastically heterogeneous systems, called Eshelby's argument [33,37,38]. On the other hand, when two (iv) or three (vii) adsorbed sites are located on the NNN sites, the enthalpy decreases by 0.05–0.1 per site compared to two isolated adsorbed sites. This implies that the effective interactions induced by the host's elasticity give rise to the formation of a 1/3-filling SL. In more detail, the contribution of the enthalpy change can be divided into the NN elastic interaction, the NNN elastic interaction, and the global pressure term $P\Delta V$. As shown in Fig. 3(b), the NN elastic interaction favors forming a connected cluster [(ii), (v), (vi)]. However, as shown in Fig. 3(c), the NNN elastic interactions raise the energy when adsorbed sites form a cluster and lower the energy when they are placed at NNN sites. Thus, the NNN elastic interaction is responsible for the formation of the 1/3-filling SL adsorbed state. We note that local configuration (iii), a base of the 2×2 (1/4-filling) SL state observed in experimentally [19,21,22,29], is not favored by either NN or NNN elastic interactions. This tendency does not change in the guest-induced lattice contraction case [see Supplemental Material Figs. S3(d)–S3(f) [36]].

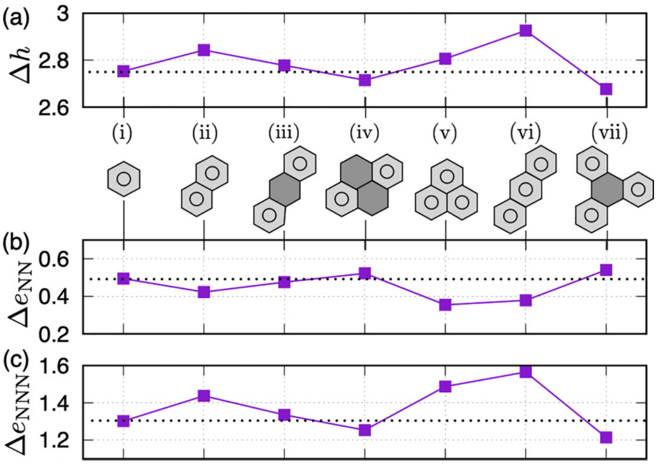

FIG. 3. (a) The enthalpy difference per adsorbed sites $\Delta h = H/N_{\text{ads}}$ between the ground state at $(\mu, P) = (0, 0.5)$ and the selected configurations [(i)–(vii)] for $k = 3$, $\alpha = 0.4$, $g = 1$, and $L = 24$. The lattice sites are optimized by MC simulations at $T = 0$ for 10^4 MC steps. Circles denote the adsorbates, and open hexagons denote the desorbed sites. (b) Δe_{NN} and (c) Δe_{NNN} represent the contributions of the NN and NNN elastic interactions to the enthalpy difference shown in (a), respectively.

The NNN interaction must be sufficiently large for the 1/3-filling SL state to be globally stable. Unlike the above enthalpy comparison under fixed guest particle number conditions, the number of guest particles in our MC simulations is variable by changing the chemical potential μ and temperature T. When μ is small, the desorbed state is the most stable because of its small lattice deformation. On the other hand, as μ is increased, a fully adsorbed state, which has three times the number of adsorbed sites of the SL state, is stabilized. For the SL state to be stabilized instead of these two competing states in the intermediate μ region, the enthalpy difference between the cluster of adsorption sites and the SL alignment must be sufficiently large. Because Δe_{NNN} is enhanced, the SL state emerges for $g = 2$, but not for $g = 1$ (see Fig. 2).

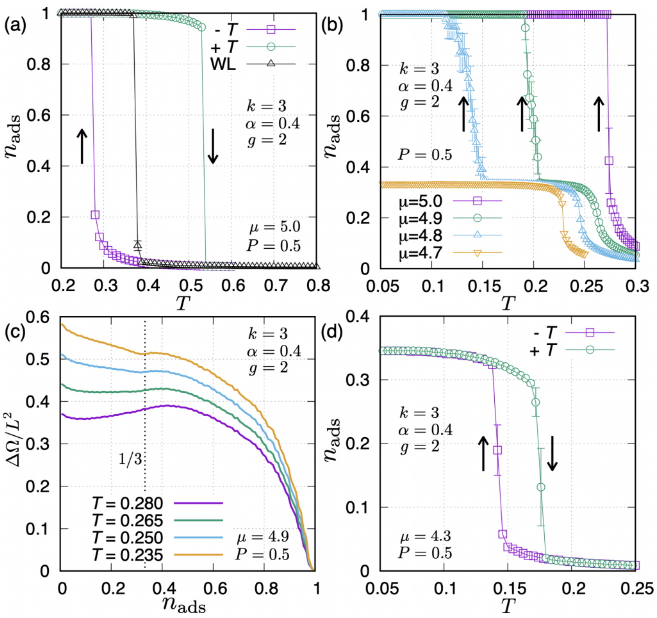

FIG. 4. Thermodynamic properties at $P = 0.5$ in the case of $k = 3$, $\alpha = 0.4$, and $g = 2$. (a) Temperature dependency of the adsorption fraction n_{ads} at $\mu = 5.0$, obtained by the WL simulation for $L = 12$, and cooling $(-T)$ and heating $(+T)$ simulations for $L = 48$. (b) $1/3$ plateau behaviors of n_{ads} at $\mu = 5.0$–4.7 during the cooling protocols. Curves at $\mu = 4.8, 4.9$ are simulated for $L = 72$, otherwise $L = 48$. (c) The osmotic grand potential $\Delta\Omega(n_{\mathrm{ads}}) = \Omega(n_{\mathrm{ads}}) - \Omega_{\mathrm{min}}$ at $T = 0.280$–0.235 and $\mu = 4.9$ for $L = 12$, where Ω_{min} is the minimum value at each T. (d) Temperature dependency of n_{ads} at $\mu = 4.3$, obtained by cooling $(-T)$ and heating $(+T)$ simulations for $L = 48$. The error bars in (a), (b), and (d) represents the standard error.

To examine the thermodynamic properties and metastability, we next calculate the temperature dependency of the adsorption fraction $n_{\mathrm{ads}} = N_{\mathrm{ads}}/L^2 = \frac{1}{L^2}\sum_{\hexagon=1}^{L^2}\sigma_{\hexagon}$, which is an order parameter of this system. In the following, we show the MC results for $g = 2$, corresponding to the phase diagram shown in Fig. 2(b). Figure 4(a) shows the temperature dependency of n_{ads} at $\mu = 5.0$ crossing the red, yellow, and blue regions in the phase diagram [Fig. 2(b)]. In the standard MC simulations, the transition between the adsorbed and desorbed states exhibits large hysteresis, quite similar to the one observed in the square lattice model [34]. In sharp contrast, as shown in Fig. 4(b), n_{ads} exhibits a $1/3$ plateau and two-step growth during the cooling protocol at $\mu = 4.9$, 4.8, and 4.7 crossing the dark gray region in the phase diagram, while n_{ads} decreases by one step during the heating protocol (see Supplemental Material Fig. S4 [36]). This implies that the $1/3$-filling SL state is metastable in a certain range of temperature and chemical potential. The plateau has a slight slope, which can be interpreted as a change in the number of vacancy defects in the SL (see also Supplemental Material Fig. S2 [36]). A clean $1/3$-filling SL is observed at low temperatures, while many vacancy defects appear at high temperatures. The metastability of the $1/3$-filling SL state can be observed in the osmotic grand potential landscape $\Omega(n_{\mathrm{ads}})$ against the adsorption fraction. The case of $\mu = 4.9$ is shown in Fig. 4(c). The local minimum shifts from $n_{\mathrm{ads}} \approx 0$ to a value slightly smaller than $n_{\mathrm{ads}} = 1/3$ as the temperature is lowered, which agrees with the intermediate plateau in Fig. 4(b). The gradual shift of the local minima also corresponds to the slight slope of the plateau. This implies that the vacancy defects entropically contribute to the osmotic grand potential. We note that it is difficult to perform the WL simulation below $\mu = 4.8$ due to the huge numerical cost. It is also observed that a hysteretic behavior between two metastable states, $1/3$-filling SL and desorbed states, emerges. Figure 4(d) shows the temperature dependency of n_{ads} at $\mu = 4.3$ crossing the light gray region in the phase diagram shown in Fig. 2(b). One can find that the hysteresis appears in a certain temperature range, from $T = 0.142$ to 0.176. This implies that there is a thermodynamic free-energy barrier between the $1/3$-filling SL state, and the SL state is robust against thermal fluctuation below $T = 0.176$. Thus, it is confirmed that the $1/3$-filling SL state exists in the finite parameter region as a metastable state.

In summary, we have shown that a long-range ordered $\sqrt{3} \times \sqrt{3}$ (1/3-filling) SL state emerges when NNN elastic interactions are strong. The elastic energy of the SL arrangement is less than one of the fully adsorbed state, which becomes the dominant effect compared to the chemical potential. We have constructed the flexible honeycomb lattice model, incorporating lattice expansion and hardening, and performed standard and multicanonical MC simulations. The phase behavior of this model has been studied. As a result, the long-range ordered $1/3$-filling SL state has been obtained by the cooling simulation. Furthermore, by calculating the thermodynamic stability, it has been found that the $1/3$-filling SL is robust against thermal fluctuation.

We discuss the reasons for the difference between the SL pattern observed experimentally [19,21,22,29] and the one obtained by our simulations. In an experimental system, IRMOF-74-V-hex, it has been explained that the lattice distortion is caused by capillary condensation of guest particles in the pores. MD simulations [20] have shown that the lattice distortion forms a structure in which regular hexagonal pores with a higher adsorbate density are surrounded by anisotropically distorted pores with a lower adsorbate density, which is consistent with the 2×2 SL pattern. The surrounding pores form a spiral shape around the regular hexagon. This is because the metallic nodes have a helical structure with three times pitch in the direction perpendicular to the honeycomb plane. The helical angle of metallic nodes corresponds to the one of hexagons forming the honeycomb structure. Each angle of the helix is changed upon adsorption, leading to the twisted distortion. Thus, the distortion pattern in IRMOF-74-V-hex is favored due to the local mechanical properties of the pore, which depend on how the metal ions and organic linkers are connected. Such an anisotropy is not incorporated into our model. The above argument suggests that the pattern of the SL structure can change depending on the local elastic properties, for example, a $\sqrt{3} \times \sqrt{3}$ SL is formed if the isotropic expansion is favored with strong NNN elastic interactions, and a 2×2 SL is formed if anisotropically twisted strains would be favored.

Finally, we discuss the possible applications of adsorbate SLs. Unlike the SLs in other condensed matter [23–28], the number of adsorbed molecules is variable; then the adsorbate SLs in SPCs undergo the transitions to homogeneous states depending on the temperature and chemical potential. This property is utilized for the switching of the magnetism and conductivity of MOFs as well as optical and phononic properties. In magnetic MOFs, the superexchange interaction between magnetic moments is modulated by the adsorption of oxygen or nitrogen molecules. Magnetic switching utilizing this modulation has been proposed both experimentally and theoretically [39,40]. Thus, the formation of intermediate SL states can be utilized for multistep magnetic switching. Furthermore, some MOFs exhibit semiconductor behavior [41]. The periodic potentials induced from the SL may modulate the conductor band structures of semimetal MOFs, which can lead to the transition to metals or insulators. Thus, the adsorbate SL states are expected to be utilized for magnetic/electric sensor devices.

This work was supported by KAKENHI Grant No. JP20H05619 from MEXT, Japan.

---

[1] S. Horike, S. Shimomura, and S. Kitagawa, Soft porous crystals, Nat. Chem. **1**, 695 (2009).

[2] H. Furukawa, K. E. Cordova, M. O'Keeffe, and O. M. Yaghi, The chemistry and applications of metal-organic frameworks, Science **341**, 1230444 (2013).

[3] Y. A. Mezenov, A. A. Krasilin, V. P. Dzyuba, A. Nominé, and V. A. Milichko, Metal–organic frameworks in modern physics: Highlights and perspectives, Adv. Sci. **6**, 1900506 (2019).

[4] J.-R. Li, J. Sculley, and H.-C. Zhou, Metal–organic frameworks for separations, Chem. Rev. **112**, 869 (2012).

[5] L. E. Kreno, K. Leong, O. K. Farha, M. Allendorf, R. P. Van Duyne, and J. T. Hupp, Metal–organic framework materials as chemical sensors, Chem. Rev. **112**, 1105 (2012).

[6] A. Bavykina, N. Kolobov, Il Son Khan, J. A. Bau, A. Ramirez, and J. Gascon, Metal–organic frameworks in heterogeneous catalysis: Recent progress, new trends, and future perspectives, Chem. Rev. **120**, 8468 (2020).

[7] P. Horcajada, R. Gref, T. Baati, P. K. Allan, G. Maurin, P. Couvreur, G. Férey, R. E. Morris, and C. Serre, Metal–organic frameworks in biomedicine, Chem. Rev. **112**, 1232 (2012).

[8] S. Krause, N. Hosono, and S. Kitagawa, Chemistry of soft porous crystals: Structural dynamics and gas adsorption properties, Angew. Chem., Int. Ed. **59**, 15325 (2020).

[9] A. U. Ortiz, A. Boutin, A. H. Fuchs, and F.-X. Coudert, Investigating the pressure-induced amorphization of zeolitic imidazolate framework ZIF-8: Mechanical instability due to shear mode softening, J. Phys. Chem. Lett. **4**, 1861 (2013).

[10] S. Henke, W. Li, and A. K. Cheetham, Guest-dependent mechanical anisotropy in pillared-layered soft porous crystals – a nanoindentation study, Chem. Sci. **5**, 2392 (2014).

[11] F. Mouhat, D. Bousquet, A. Boutin, L. Bouëssel du Bourg, F.-X. Coudert, and A. H. Fuchs, Softening upon adsorption in microporous materials: A counterintuitive mechanical response, J. Phys. Chem. Lett. **6**, 4265 (2015).

[12] P. Canepa, K. Tan, Y. Du, H. Lu, Y. J. Chabal, and T. Thonhauser, Structural, elastic, thermal, and electronic responses of small-molecule-loaded metal–organic framework materials, J. Mater. Chem. A **3**, 986 (2015).

[13] C. Serre, S. Bourrelly, A. Vimont, N. A. Ramsahye, G. Maurin, P. L. Llewellyn, M. Daturi, Y. Filinchuk, O. Leynaud, P. Barnes, and G. Férey, An explanation for the very large breathing effect of a metal–organic framework during CO_2 adsorption, Adv. Mater. **19**, 2246 (2007).

[14] H. J. Choi, M. Dincă, and J. R. Long, Broadly hysteretic H_2 adsorption in the microporous metal–organic framework Co(1,4-benzenedipyrazolate), J. Am. Chem. Soc. **130**, 7848 (2008).

[15] F. Salles, G. Maurin, C. Serre, P. L. Llewellyn, C. Knofel, H. J. Choi, Y. Filinchuk, L. Oliviero, A. Vimont, J. R. Long, and G. Férey, Multistep N_2 breathing in the metal–organic framework Co(1,4-benzenedipyrazolate), J. Am. Chem. Soc. **132**, 13782 (2010).

[16] C. O. Ania, E. García-Pérez, M. Haro, J. J. Gutiérrez-Sevillano, T. Valdés-Solís, J. B. Parra, and S. Calero, Understanding gas-induced structural deformation of ZIF-8, J. Phys. Chem. Lett. **3**, 1159 (2012).

[17] S. Krause, J. D. Evans, V. Bon, I. Senkovska, P. Iacomi, F. Kolbe, S. Ehrling, E. Troschke, J. Getzschmann, D. M. Többens *et al.*, Towards general network architecture design criteria for negative gas adsorption transitions in ultraporous frameworks, Nat. Commun. **10**, 3632 (2019).

[18] F.-X. Coudert and A. H. Fuchs, Computational characterization and prediction of metal–organic framework properties, Coord. Chem. Rev. **307**, 211 (2016).

[19] H. S. Cho, H. Deng, K. Miyasaka, Z. Dong, M. Cho, A. V. Neimark, J. K. Kang, O. M. Yaghi, and O. Terasaki, Extra adsorption and adsorbate superlattice formation in metal-organic frameworks, Nature (London) **527**, 503 (2015).

[20] S. Jawahery, C. M. Simon, E. Braun, M. Witman, D. Tiana, B. Vlaisavljevich, and B. Smit, Adsorbate-induced lattice deformation in IRMOF-74 series, Nat. Commun. **8**, 13945 (2017).

[21] M. I. Gonzalez, M. T. Kapelewski, E. D. Bloch, P. J. Milner, D. A. Reed, M. R. Hudson, J. A. Mason, G. Barin, C. M. Brown, and J. R. Long, Separation of xylene isomers through multiple metal site interactions in metal–organic frameworks, J. Am. Chem. Soc. **140**, 3412 (2018).

[22] B. Pato-Doldán, M. H. Rosnes, D. Chernyshov, and P. D. C. Dietzel, Carbon dioxide induced structural phase transition in metal–organic frameworks CPO-27, CrystEngComm **22**, 4353 (2020).

[23] T. C. Harman, P. J. Taylor, M. P. Walsh, and B. E. LaForge, Quantum dot superlattice thermoelectric materials and devices, Science **297**, 2229 (2002).

[24] A. A. Balandin and O. L. Lazarenkova, Mechanism for thermoelectric figure-of-merit enhancement in regimented quantum dot superlattices, Appl. Phys. Lett. **82**, 415 (2003).

[25] J. Stangl, V. Holý, and G. Bauer, Structural properties of self-organized semiconductor nanostructures, Rev. Mod. Phys. **76**, 725 (2004).

[26] J. N. Aqua, I. Berbezier, L. Favre, T. Frisch, and A. Ronda, Growth and self-organization of SiGe nanostructures, Phys. Rep. **522**, 59 (2013).

[27] F. P. G. de Arquer, D. V. Talapin, V. I. Klimov, Y. Arakawa, M. Bayer, and E. H. Sargent, Semiconductor quantum dots:

Technological progress and future challenges, Science **373**, eaaz8541 (2021).

[28] D. García-Lojo, S. Núñez-Sánchez, S. Gómez-Graña, M. Grzelczak, I. Pastoriza-Santos, J. Pérez-Juste, and L. M. Liz-Marzán, Plasmonic supercrystals, Acc. Chem. Res. **52**, 1855 (2019).

[29] M. Jansen, W. A. Tisdale, and V. Wood, Nanocrystal phononics, Nat. Mater. **22**, 161 (2023).

[30] R. J. Asaro and W. A. Tiller, Interface morphology development during stress corrosion cracking: Part I. via surface diffusion, Metall. Trans. **3**, 1789 (1972).

[31] M. A. Grinfeld, Instability of the interface between a nonhydrostatically stressed elastic body and a melt, Sov. Phys. Dokl. **31**, 831 (1986).

[32] P. Politi, G. Grenet, A. Marty, A. Ponchet, and J. Villain, Instabilities in crystal growth by atomic or molecular beams, Phys. Rep. **324**, 271 (2000).

[33] A. Onuki, *Phase Transition Dynamics* (Cambridge University Press, Cambridge, UK, 2002).

[34] K. Mitsumoto and K. Takae, Elastic heterogeneity governs asymmetric adsorption–desorption in a soft porous crystal, Proc. Natl. Acad. Sci. USA **120**, e2302561120 (2023).

[35] F.-X. Coudert, M. Jeffroy, A. H. Fuchs, A. Boutin, and C. Mellot-Draznieks, Thermodynamics of guest-induced structural transitions in hybrid organic-inorganic frameworks, J. Am. Chem. Soc. **130**, 14294 (2008).

[36] See Supplemental Material at http://link.aps.org/supplemental/10.1103/PhysRevResearch.6.L012029 for details of numerial simulations and extended figures.

[37] A. G. Khachaturyan, *Theory of Structural Transformations in Solids* (Wiley, New York, 1983).

[38] J. D. Eshelby, The determination of the elastic field of an ellipsoidal inclusion, and related problems, Proc. R. Soc. London, Ser. A **241**, 376 (1957).

[39] W. Kosaka, Z. Liu, J. Zhang, Y. Sato, A. Hori, R. Matsuda, S. Kitagawa, and H. Miyasaka, Gas-responsive porous magnet distinguishes the electron spin of molecular oxygen, Nat. Commun. **9**, 5420 (2018).

[40] M. Kato, K. Tokushuku, H. Matsuura, M. Udagawa, and M. Ogata, Magnetic switching by oxygen adsorption in metal–organic framework systems, J. Phys. Soc. Jpn. **90**, 073704 (2021).

[41] M. Alvaro, E. Carbonell, B. Ferrer, F. X. L. i Xamena, and H. Garcia, Semiconductor behavior of a metal–organic framework (MOF), Chem. Eur. J. **13**, 5106 (2007).